2026 InterPore

A model for seasonal energy storage in cone-shaped geological formations

Hatem ALAMARA[1], Igor BOGDANOV[1], Sabine DELAHAYE[2]
[1] CHLOE Research Laboratory, [2] TotalEnergies CSTJF, Pau, France

1. Context and objectives

We study the dynamics of cyclic currents when a fluid is repeatedly injected and produced in an inclined, radially-symmetric porous formation, a situation typical of underground gas or thermal aquifer storage in geological structures. These cycles generate time-dependent interface evolution governed mainly by both advection and buoyancy. Our aim is to model the current's behavior, identify the controlling dimensionless groups, and characterize the flow's equilibrium and scaling laws for operational optimization. A distinctive feature of the present model is that it investigates a geometry that has not been thoroughly researched analytically before [1-4] and provides closed form expressions when possible.

2. Mathematical description

We idealize three-dimensional anticlinal or synclinal geological structures by a conical, axisymmetric domain (Fig. 1) and assume homogeneous-acting petrophysical properties, hydrostatic pressure distribution, negligible variation in fluid properties, and vertical segregation between phases. Under these assumptions, we derive a depth-averaged PDE governing the evolution of the injected fluid layer during cyclic operation which represent the first result of this study:

$$\left(\sigma=\begin{cases}1, & S_n^{max}=0\\ \dfrac{1-S_{nm}-S_{wm}}{1-S_{wm}}, & S_n^{max}>0\end{cases}\right)\cdot\frac{\partial S_n}{\partial t}+\frac{1}{r}\frac{\partial}{\partial r}\left[\left(\frac{\mathcal{M}K_{rn}}{\mathcal{M}K_{rn}+K_{rw}}\right)\left(\Xi-N_b K_{rw} r\left(N_s+\frac{\partial z_c}{\partial r}\right)\right)\right]=0.$$

Here, S_n is the normalized depth-averaged saturation of the injected phase, K_{rj} are the normalized depth-averaged relative permeabilities, z_c is the dimensionless contact depth between the phases. The governing dimensionless numbers are listed in Table. 1. The injection–production cycle is imposed through the following boundary flux, in which production stops once $S_n(r_i=1,t)=0$:

$$F(r_i=1,t)=\Xi(t)\quad\text{where}\quad \Xi(t)=\left(\begin{cases}+1, & 2(n-1)\Omega\le t\le(2n-1)\Omega \quad \text{(Inj)}\\ -1, & (2n-1)\Omega<t<2n\Omega \quad \text{(Prod)}\end{cases}\right)\cdot 1_{\{S_n(r_i=1,t)>0\}}.$$

The depth-averaged flow functions corresponding to the Brooks-Corey-Burdine fine-scale model are obtained analytically as functions of the contact depth z_c, Bond number $\mathcal{B}o$, and pore size distribution exponent λ:

$$S_n(z_c;\mathcal{B}o,\lambda)=\boldsymbol{z_c}-I\big(\lambda;\sigma(z_c)\big),\qquad K_{rw}(z_c;\mathcal{B}o,\lambda)=\mathbf{1}-\boldsymbol{z_c}+I\big(3\lambda+2;\sigma(z_c)\big),$$
$$K_{rn}(z_c;\mathcal{B}o,\lambda)=\boldsymbol{z_c}-2I\big(\lambda;\sigma(z_c)\big)+I\big(2\lambda;\sigma(z_c)\big)-I\big(\lambda+2;\sigma(z_c)\big)+2I\big(2\lambda+2;\sigma(z_c)\big)-I\big(3\lambda+2;\sigma(z_c)\big),$$

where the auxiliary functions: $I\big(\xi;\sigma(z_c)\big):=\frac{1}{\mathcal{B}o}\begin{cases}\frac{1-(1+\mathcal{B}o\cdot\sigma)^{1-\xi}}{\xi-1}, & \xi\neq 1\\ \ln(1+\mathcal{B}o\cdot\sigma), & \xi=1\end{cases}$, $\sigma(z_c)=\min(z_c,\delta)$, $\delta=\frac{p_c^m-1}{\mathcal{B}o}$.

On the other hand, the pressure perturbation at a reference surface can be computed once the fluid's layer thickness is obtained using:

$$r\frac{\partial\Delta p_n}{\partial r}=\frac{N_b}{(\mathcal{M}K_{rn}+K_{rw})}\left[rN_s(\mathcal{M}K_{rn}\gamma_n+K_{rw}\gamma_w)-\mathcal{M}K_{rn}r\frac{\partial z_c}{\partial r}-\frac{\Xi}{N_b}\right].$$

3. Stability criterion

The conical geometry admits a simple criterion expressed as a critical radius beyond which the flow becomes approximately gravity-stabilized:

$$r_{cr}=\frac{\mathcal{M}-1}{\mathcal{M}N_bN_s}\quad\rightarrow\quad r_{cr}^*=\left(\frac{\mu_w}{k_{rw}^e}-\frac{\mu_n}{k_{rn}^e}\right)\frac{Q}{2\pi Hk_x\Delta\gamma^*\sin\theta}.$$

For UHS in aquifer, the expected range is $O(10^0-10^3)$ m. This criterion is the conical-geometry counterpart of the classical Dietz condition [5].

4. Gravity-stabilized solutions

Exact analytical expressions for gravity-stabilized flows were derived and are presented with a numerical example in Fig. 2. These solutions represent the most favorable recovery scenario, in which the flow relaxes toward its gravity-dominated steady profile during each stage. Under these conditions, the recovery improves geometrically from cycle to cycle, while the incremental residually trapped mass declines geometrically. After only a few cycles, the system approaches a quasi-equilibrium cyclic state. For such flows, the only irrecoverable mass is that residually trapped: $W_\infty=\frac{M_\infty^{res}}{\Omega}=\left(\frac{1-\sigma_h}{\sigma_h}\right)$ as $n\rightarrow\infty$.

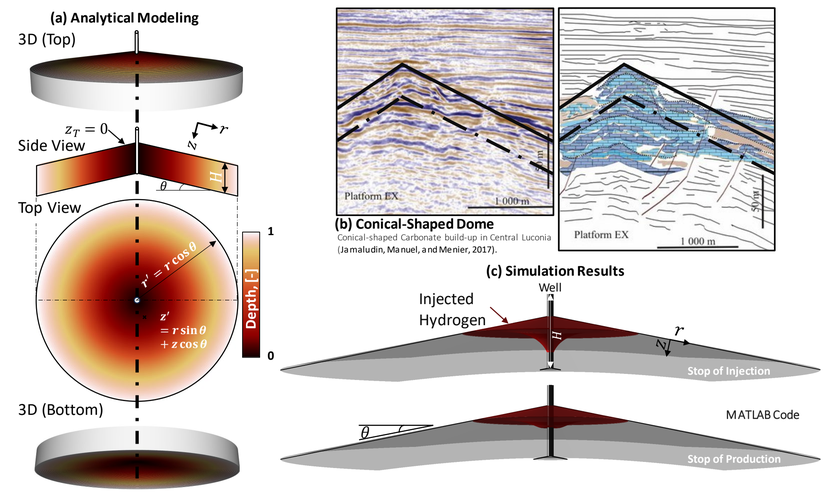

Fig. 1 — Conceptual modeling, conical shaped dome, and sample simulation results.

Tab. 1 — Governing dimensionless groups.

Trapping number	$\sigma_h=\frac{S_{nM}^{imb}}{S_{nm}^{drg}}=\frac{1-S_{nm}-S_{wm}}{1-S_{wm}}$
Cycling frequency	$\Omega=\left(u_b=\frac{k_{rn}^e k_x\Delta\gamma^*\cos\theta}{\mu_n}\right)^2\frac{2\pi Ht_{1/2}^*}{\phi_r^* s_{nM}^{drg}Q}$
Buoyancy number	$N_b=\frac{2\pi H^2k_{rw}^e k_x\Delta\gamma^*\cos\theta}{Q\mu_w}$
Slope number	$N_s=\frac{r_c}{H}\tan\theta=\frac{Q\mu_n}{2\pi H^2k_{rn}^e k_x\Delta\gamma^*}\sec\theta\tan\theta$
Mobility ratio	$\mathcal{M}=\left(\frac{k_{rn}^e}{k_{rw}^e}\right)\left(\frac{\mu_w}{\mu_n}\right)$
Bond number	$\mathcal{B}o=\frac{\Delta\gamma^*H\cos\theta}{p_e}$
Pore-distribution exp.	λ

Mobile Mass

$$\boldsymbol{M_N^{mob}(t)}=\begin{cases}\dfrac{t-2(n-1)\Omega}{\sigma\Omega}, & 2(n-1)\Omega\le t\le t_{r,n}\\ B_{n-1}+\dfrac{t}{\Omega}-2(n-1), & t_{r,n}<t\le(2n-1)\Omega\\ A_n-\dfrac{t-(2n-1)\Omega}{\sigma\Omega}, & (2n-1)\Omega\le t\le t_{d,n}\\ 0, & t_{d,n}<t\le 2n\Omega\end{cases}.$$

Residual Mass

$$\boldsymbol{M_N^{res}(t)}=\begin{cases}B_{n-1}-\left(\dfrac{1-\sigma_h}{\sigma_h}\right)\left[\dfrac{t}{\Omega}-2(n-1)\right], & 2(n-1)\Omega\le t\le t_{r,n}\\ 0, & t_{r,n}<t\le(2n-1)\Omega\\ \left(\dfrac{1-\sigma_h}{\sigma_h}\right)\left[\dfrac{t}{\Omega}-(2n-1)\right], & (2n-1)\Omega\le t\le t_{d,n}\\ B_n, & t_{d,n}<t\le 2n\Omega\end{cases}.$$

Total Mass

$$\boldsymbol{M_N^{tot}(t)}=\begin{cases}B_{n-1}+\dfrac{t}{\Omega}-2(n-1), & 2(n-1)\Omega\le t\le(2n-1)\Omega,\\ A_n-\left[\dfrac{t}{\Omega}-(2n-1)\right], & (2n-1)\Omega\le t\le t_{d,n},\\ B_n, & t_{d,n}<t\le 2n\Omega.\end{cases}$$

Leading Front

$$\boldsymbol{r_f^+(t)}=\begin{cases}\left(\dfrac{6\Omega M_N^{mob}}{N_s}\right)^{1/3}, & M_N^{mob}\le\dfrac{1}{6\Omega N_s^2},\\ \dfrac{3+\sqrt{72N_s^2\Omega M_N^{mob}-3}}{6N_s}, & M_N^{mob}>\dfrac{1}{6\Omega N_s^2}.\end{cases}$$

Trailing Front

$$\boldsymbol{r_f^-(t)}=r_f^+-\frac{1}{N_s}.$$

Mobile Interface

$$\boldsymbol{z_c(r,t)}=\begin{cases}N_s(r_f^+-r), & 0\le r\le r_f^+\\ 0, & r\ge r_f^+\end{cases},\qquad M_N^{mob}\le\frac{1}{6\Omega N_s^2},$$
$$\boldsymbol{z_c(r,t)}=\begin{cases}1, & 0\le r\le r_f^-\\ N_s(r_f^+-r), & r_f^-<r\le r_f^+\\ 0, & r>r_f^+\end{cases},\qquad M_N^{mob}>\frac{1}{6\Omega N_s^2}.$$

Mass peaks: $\boldsymbol{A_n}=\frac{1}{\sigma}[1-(1-\sigma)^n]$.

Mass troughs: $\boldsymbol{B_n}=\left(\frac{1-\sigma}{\sigma}\right)[1-(1-\sigma)^n]$.

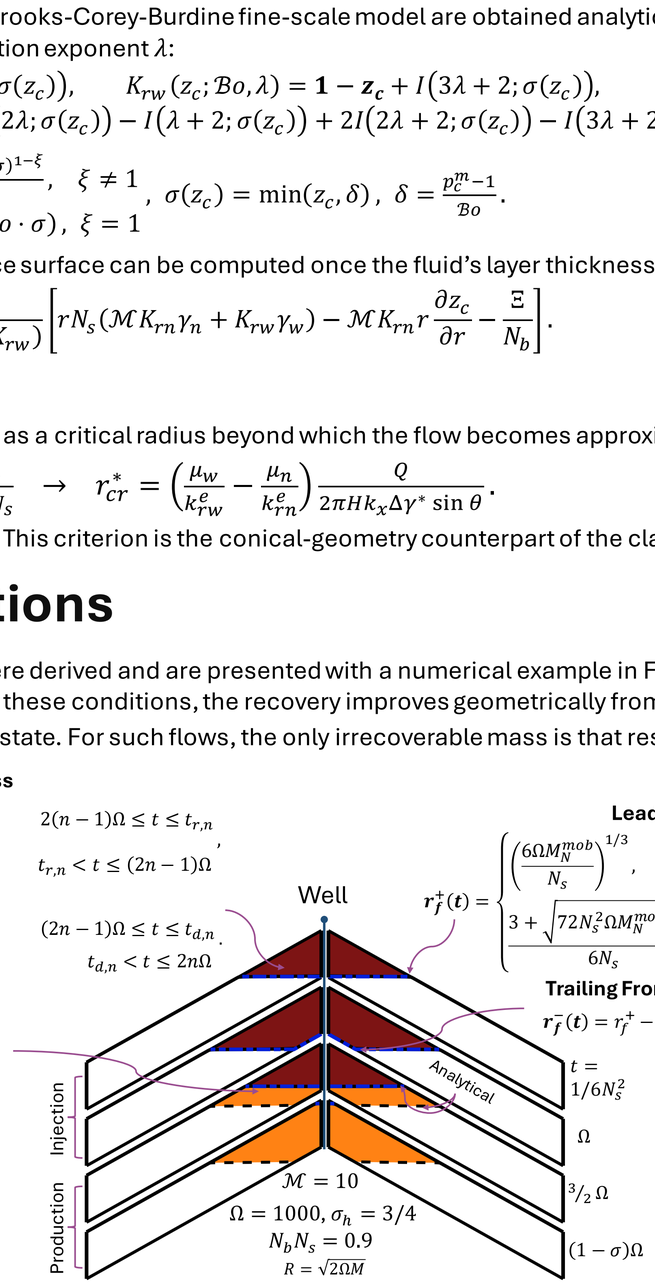

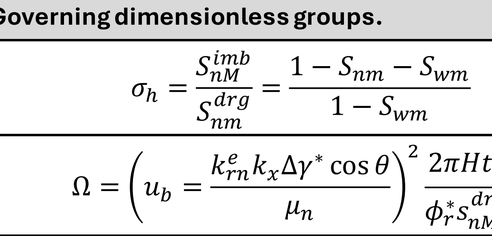

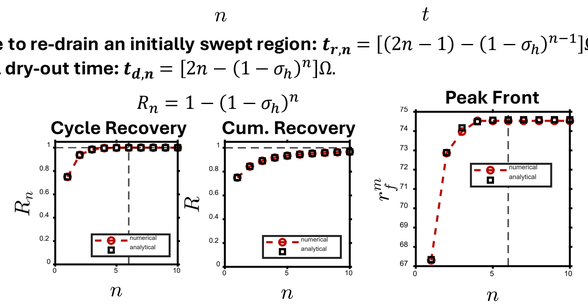

Time to re-drain an initially swept region: $\boldsymbol{t_{r,n}}=[(2n-1)-(1-\sigma_h)^{n-1}]\Omega$.
Well dry-out time: $\boldsymbol{t_{d,n}}=[2n-(1-\sigma_h)^n]\Omega$.

$R_n=1-(1-\sigma_h)^n$

Fig. 2 — Gravity-stabilized flow: numerical simulation and analytical expressions.

5. Unstable flow and capillarity

Unstable flow is more involved, and no general exact solution was obtained. Nevertheless, the system still tends toward a quasi-equilibrium state over successive cycles. The irrecoverable mass is larger than in the gravity-stabilized limit because additional injected mass becomes dynamically trapped once the well produces mainly the initially resident phase. The quasi-equilibrium cushion-to-working gas ratio can be approximated by

$$W_\infty\approx\left(\frac{1-\sigma_h}{\sigma_h}\right)+\frac{M_{dyn}^{trap}}{\Omega}.$$

Capillarity increases dynamic trapping by reducing mobility near the leading edge of the front (Fig. 3). As far as pressure is concerned, production requires a larger pressure perturbation than injection of the same mass.

To interpret the trends in W_∞, equilibrium cycle n_∞, and peak front r_f^∞, we generated a large set of numerical experiments (using Latin Hypercube Sampling), summarized in Fig. 4 below.

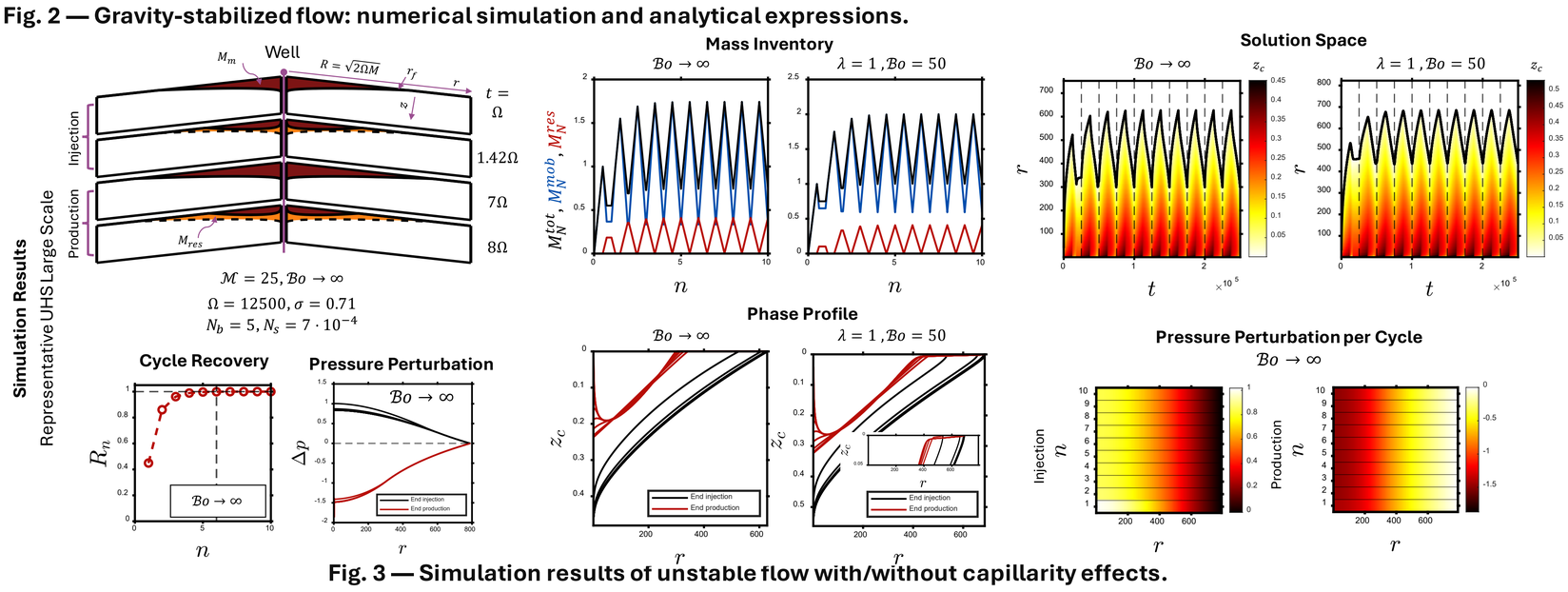

Fig. 3 — Simulation results of unstable flow with/without capillarity effects.

6. Conclusions

- An analytical framework was developed for cyclic seasonal storage in an underexplored cone-shaped geological geometry, with hydrogen storage in aquifers used as a representative application.
- A reduced dimensionality MATLAB code was developed to study stable and unstable cyclic displacements including hysteresis and capillary effects.
- Stability analysis provides a critical-radius criterion and exact analytical expressions for gravity-stabilized flows. This offers a direct physical insight into the role of geometry, buoyancy, and mobility contrast.
- Both stable and unstable displacements tend toward a quasi-equilibrium cyclic state. However, unstable displacements require more cycles to reach equilibrium and lead to larger irrecoverable fractions of the injected phase.
- In gravity-stabilized flows, the only irrecoverable mass is that residually trapped; this residual mass approaches its quasi-steady value geometrically, while recovery improves geometrically over cycles.
- Operational constraints may dynamically strand more mass than residual trapping alone.
- For unstable flows, the simulation experiments show that the irrecoverable mass and the time to equilibrium decrease with $\mathcal{M}(N_bN_s)^2\Omega$, while the peak front position increases with the same composite group.

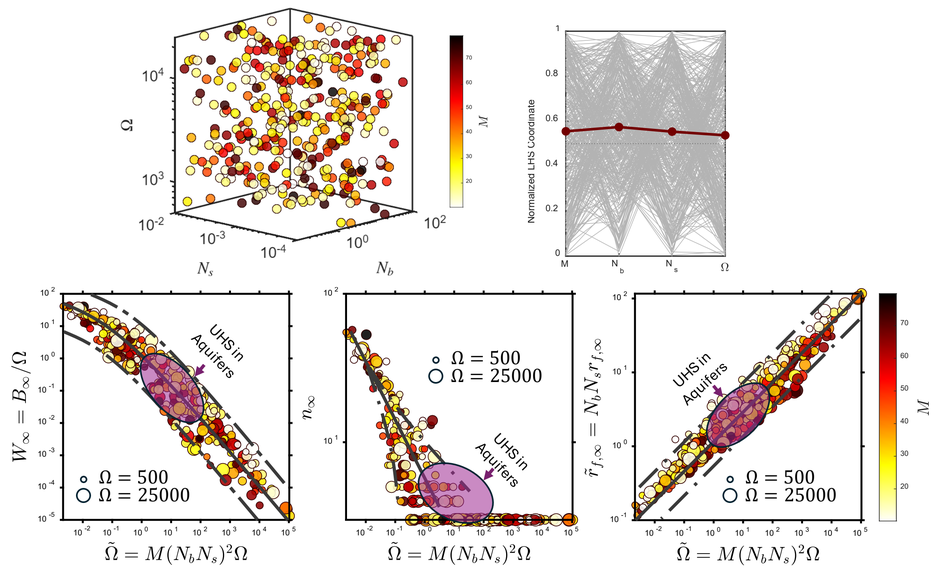

Fig. 4 — Top: LHS experiments space. Bottom: trends of cushion-to-working mass ratio, equilibrium cycle, and peak front at equilibrium.

7. References

[1] Dudfield & Woods, J. Fluid Mech., 755, 111–141, 2014. **[2]** Whelan & Woods, J. Fluid Mech., 1002, R2, 2025. **[3]** Nordbotten & Celia, J. Fluid Mech., 561, 307–327, 2006. **[4]** Rabinovich, J. Hydrol., 570, 682–691, 2019. **[5]** Dietz, Proc. K. Ned. Akad. Wet., 56-B, 83–92, 1953. **[6]** Jamaludin et al., J. Earth Sci., 29, 155–168, 2018.